Optimal Sampling Frequency and Bias Error Modeling for Foot-Mounted IMUs

Estefania Munoz Diaz, Oliver Heirich, Mohammed Khider and Patrick Robertson
German Aerospace Center (DLR)
Institute of Communications and Navigation
Oberpfaffenhofen, 82234 Wessling, Germany
Email: {Estefania.Munoz, Oliver.Heirich, Mohammed.Khider, Patrick.Robertson}@dlr.de

***Abstract*—The use of foot-mounted inertial measurement units (IMUs) has shown promising results in providing accurate human odometry as a component of accurate indoor pedestrian navigation. The specifications of these sensors, such as the sampling frequency have to meet requirements related to human motion.**

We investigate the lowest usable sampling frequency: To do so, we evaluate the frequency distribution of different human motion like crawling, jumping or walking in different scenarios such as escalators, lifts, on carpet or grass, and with different footwear. These measurements indicate that certain movement patterns, as for instance going downstairs, upstairs, running or jumping contain more high frequency components. When using only a low sampling rate this high frequency information is lost. Hence, it is important to identify the lowest usable sampling frequency and sample with it if possible. We have made a set of walks to illustrate the resulting odometries at different frequencies, after applying an Unscented Kalman Filter (UKF) using Zero Velocity Updates.

The odometry error is highly dependent on the drift of the individual accelerometers and gyroscopes. In order to obtain better odometry it is necessary to perform a detailed analysis of the sensor noise processes. We resorted to computing the Allan variance for three different IMU chipsets of various quality specification. From this we have derived a bias model for the UKF and evaluated the benefit of applying this model to a set of real data from walk.

I. Introduction

Positioning applications are being more important in recent years not only for security applications, but also for mass market to localization applications in shopping malls or in an airports, for example.

Most outdoors positioning applications are based on Global Navigation Satellite Systems (GNSSs), such as the american Global Positioning System (GPS) or in future the european Galileo. However, due to the lack of visible satellites, the availability of GNSS is degraded in certain scenarios such as urban canyons or indoors. The use of inertial measurement units (IMUs) is a promising solution to address this problem because they are able to provide human odometries [1]. Importantly, they are not infrastructure dependent.

However, micro electromechanical systems (MEMS) based IMUs have to face problems such as drifting sensors. Many authors [2], [3], [4], [5] used the rest phase of the foot to limit the growth of errors. Foxlin [3] was the first to use an extended Kalman filter (EKF) to estimate and substract the errors with the zero velocity updates (ZUPT) during the rest phase. There are more suitable solutions like the assumption of a fixed orientation when the sensor is in a rest phase. This is a zero angular rate update (ZARU) [2]. Recently introduced was the magnetic angular rate update (MARU) [6] that uses the changes in the magnetic field during the rest phase to detect the turn rates of the sensor. Additional sources of information, such as GPS pseudoranges [7], long-term evolution (LTE) signals [8] or barometers can be used in a sensor fusion approach [9] to aid the output of the IMU.

Nevertheless, improvements of the underlying odometry processing is still an active area of research. In the first part of this paper we study the sampling frequency that the sensor has to support to adequately capture human motion. We study different kind of surfaces such as floor tile, pavement, carpet and grass with different kind of footwear like flat shoes, sports shoes and heels. Figure 1 shows two examples of the footwear used in a set of experiments. We study as well different types of movements such as walking, running, jumping, going up- and downstairs and crawling to determine the lowest usable sampling frequency. We have done a set of walks in order to evaluate the performance at different sampling frequencies.

(a) Sports shoes (b) High heels

Fig. 1. Two examples of the footwear that have been used for the sets of experiments.

In the second part of this paper we derive an error model for estimating the bias of accelerometers and gyroscopes in order to obtain more accurate positioning results. We present the model parameters for different IMU chipsets in different tables. A set of walks were analyzed for testing the performance of the mentioned error models in the special context of foot-mounted inertial navigation. We offer as well a detailed analysis of different sensor types such as low-cost, medium range and high-end IMUs. This study is made using the Allan variance.

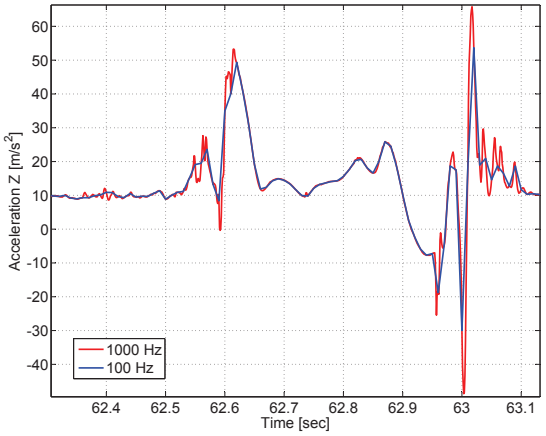

Fig. 2. Acceleration signal of a human step for the z-axis recorded with a foot-mounted IMU at 1000 Hz and at 100 Hz. We can observe parts of the signal at 1000 Hz that we lose by sampling at 100 Hz.

II. Analysis of Human Motion Sampling

Traditionally inertial sensors have been used for navigation in ships and airplanes, however with the development of the MEMS it is possible nowadays to achieve inertial pedestrian navigation.

The parameterisation of the IMU is application dependent. As a result, no universal parameters can be given. However, some groups of parameters can still be identified. In [10] a classification and study of the parameters is offered. The parameters can be divided into internal parameters and external parameters. The internal parameters can be also divided into filter parameters and hardware parameters. The parameters of the hardware set-up are only the sensor placement/mounting and the sampling frequency.

In this work we have done a study of the hardware set-up parameter sampling frequency given the sensor placement foot.

In Figure 2 the raw acceleration signal of a human step is shown. In red we can see the acceleration sampled at 1000 Hz and the blue curve represents the same data set decimated to 100 Hz. We can clearly observe the low frequency part of the human step which is present in both curves. However, there are fast variations in the acceleration that we can only see at a higher sampling rate. The high accelerations produced when the foot hists the floor, that we can see around $t = 63$ s, are pronounced only at 1000 Hz. At a lower data rate we may lose these components and the impact of losing this information is so far unknown.

A. Experimental Setup

In order to find out the lowest usable sampling frequency we have to take into account that a positioning system with foot-mounted IMUs could be used in a wide range of applications, from firemen or rescue teams to geriatrics or kindergartens. For the mass market we study staircases, ramps, elevators, escalators and moving walkway systems. For firemen we are interested in motion such as running or crawling or if we use the walking system for hospitals and geriatrics the use of zimmer frames and canes are of interest, for example.

We have performed two different experiments. For the first one we want to determine the influence of the footwear and the kind of floor. 8 different volunteers helped us, 2 children, 3 women and 3 men of different ages: 6, 3, 85, 51, 24, 28, 54 and 82 respectively. One of the women has hip prosthesis. We asked the volunteers to do a flat walk with different footwear such as flat shoes, sports shoes and heels, and different floor types as well, like floor tile, pavement, carpet and grass. The men and the children did not wear heels.

In the second set of experiments a 27 year old woman made a set of walks carrying out different motion such as walking, running, jumping, crawling and using escalators, elevators and moving walkways systems. With the idea of using different elevators, escalators and staircases we have done our experiments at three different locations: in our office building, in a shopping mall in Munich and at the Barajas airport in Madrid.

B. Methodology

We have sampled all walks for both set of experiments at 1000 Hz using the NavChip IMU of InterSense. We examine the frequenciy distribution of the raw acceleration and gyroscope signals obtained from every walk. Particularly, we compute the one-sided power spectral density (PSD). This contains the total power of the signal in the frequency interval from 0 Hz to half of the Nyquist rate, in our case from 0 Hz to 500 Hz. The PSD estimate is computed usually with a periodogram. The Welch method is an improved version of the periodogram based on averaged periodograms of overlapped windowed signal sections. We have used a Hamming window of 64 samples and a overlap factor of 50%.

In Figure 3 is shown the Welch PSD estimate of the acceleration data for all 3 axis. This is a short flat walk with a duration of about 30 seconds made by a 51 year old woman using sports shoes and walking on pavement.

The integral of the PSD over a given frequency band computes the average power in the signal over that frequency band. We have integrated the curves in Figure 3 cumulatively over the whole frequency band. Figure 4 shows the complementary cumulative distribution function (CCDF). To visualize better the significant part of the curves, we have decided to show only from 0 Hz to 300 Hz because in this particular case, we have not obtained relevant power from 300 Hz to 500 Hz.

We will assume a threshold of 95% of the total power in the CCDFs of accelerometers and gyroscopes of every walk. The corresponding sampling frequency, according to the Nyquist sampling theorem, is twice the mentioned bandwidth.

C. Experimental Results

We have analyzed in frequency domain all walks for both sets of experiments and we have discovered that the limiting signals in terms of bandwidth are those from the accelerometers. This is mostly due to the high frequencies generated when the foot hits the floor. For the gyroscopes the bandwidth

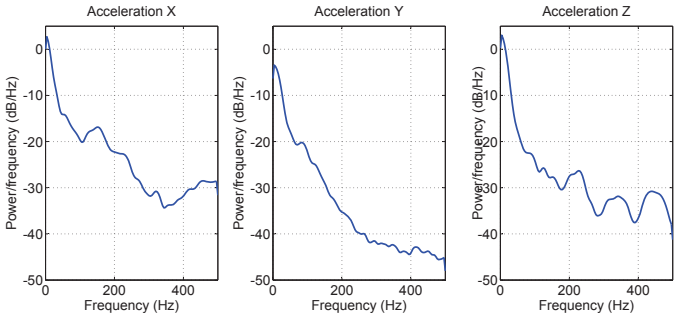

Fig. 3. Welch power spectral density estimates of accelerations X, Y and Z for a 30 seconds walk sampled at 1000 Hz.

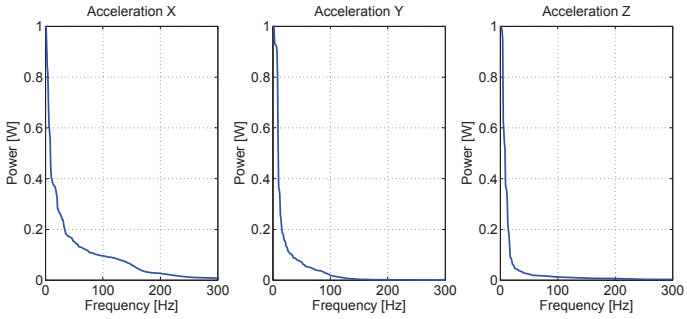

Fig. 4. Complementary cumulative distribution functions of accelerations X, Y and Z for a 30 seconds walk sampled at 1000 Hz.

needed is not greater than 50 Hz, therefore the sampling frequency would be 100 Hz.

Table I shows the required sampling frequency, in Hertz, based on the criterion explained in the previous subsection. This has been made for different kind of footwear such as flat shoes, sports shoes and heels and for different floor types like floor tile, pavement, carpet and grass. The results of all volunteers were averaged for computing the final sampling frequency.

	Floor tile	**Pavement**	**Carpet**	**Grass**
Flat shoes	200	200	200	200
Sports shoes	200	200	200	200
Heels	300	300	250	250

TABLE I
LOWEST USABLE SAMPLING FREQUENCY IN HERTZ FOR FLAT SHOES, SPORTS SHOES AND HEELS USED IN DIFFERENT FLOOR TYPES LIKE FLOOR TILE, PAVEMENT, CARPET AND GRASS.

The volunteers for this set of experiments were chosen to be representative. The 85 year old woman with hip prosthesis did some walks using a cane. The resulting needed bandwidth does not change as a result of introducing a hip prosthesis or a cane.

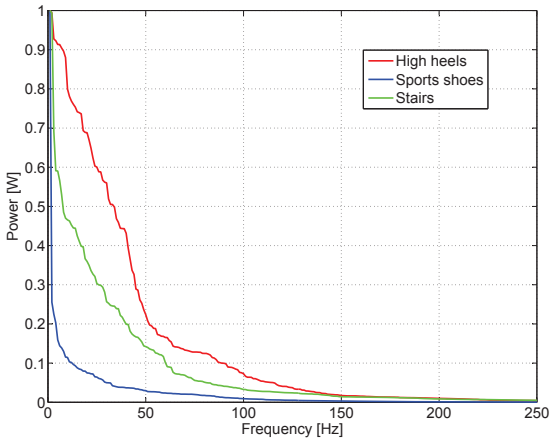

Fig. 5. Complementary cumulative distribution functions of acceleration Y for different walks sampled at 1000 Hz. In red we can see the curve of a woman wearing the high heels of Figure 1 (b) and in blue is represented the same walk wearing the sports shoes of Figure 1 (a). The green curve represents a walk using only the staircases going up and down.

We found out that the bandwidth needed for the children is slightly smaller and for men slightly greater than the average under the same conditions for all volunteers, that means using the same type of footwear and walking on the same type of floor. However, the required bandwidth is more dependent on the walking mode of the subject than on the gender.

We show the required sampling frequency, in Hertz, based on the criterion explained in the previous subsection, for the different forms of motion that have been studied. All of them have been done by the same volunteer using flat shoes. The result is the average of the same kind of walk in different scenarios.

	Escalator	**Ramp**	**Elevator**	**Walkway**
Walking	300	250	–	200
Standing	100	100	100	100

TABLE II
LOWEST USABLE SAMPLING FREQUENCY IN HERTZ FOR MECHANICAL TRANSPORTATION SYSTEMS.

Walking	**Running**	**Stairs**	**Jumping**	**Crawling**
200	300	300	350	250

TABLE III
LOWEST USABLE SAMPLING FREQUENCY IN HERTZ FOR DIFFERENT FORMS OF MOTION.

The values of TablesI, II and III were rounded to the next multiple of 50 Hz.

D. Discussion

We conclude from this study with respect to the sampling frequency that it can be considered the same for all ages and gender, however it depends a lot on the way the subject is walking.

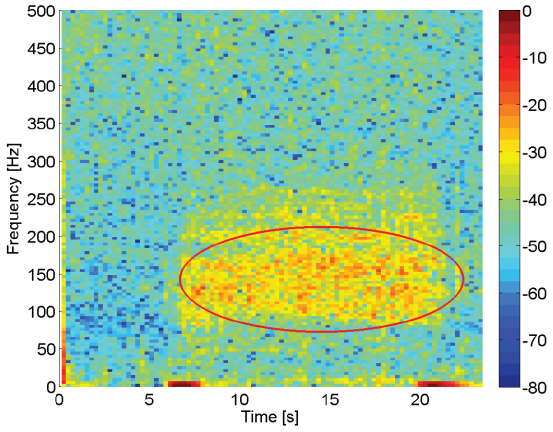

Fig. 6. Spectrogram of the raw z-axis acceleration of an elevator dataset. Since the IMU is on the foot, we can sense the motor vibration marked with a red oval.

The footwear has a big influence: by using heels there are higher frequency components produced when the shoe hits the floor (see Figure 5). In contrast, there are no remarkable differences by changing the floor type. It is clear that the softer the floor surface is, the smoother the step will be, however, it does not make difference with respect to the sampling frequency.

With respect to the different motions, we realized that when running, crawling, jumping or using staircases the sampling frequency should be higher than when walking. The variance for running, jumping and crawling is bigger because it is highly dependent of the way the user does these activities.

It should be noticed by looking at Table II that while standing or using the elevator a high sampling rate is not needed. However, we discovered that the elevator motor vibration can be measured by the sensors. It is not strictly necessary to include these vibrations in the sampling frequency, but in a general case it is likely that we need this information in order to know, for example, that we entered one of these mechanical systems and we are actually moving, not standing. We propose to modify the sampling frequency to include the motor vibration. The fundamental frequency varies with every motor. We can see an example of engine vibrations in Figure 6 where the spectrogram of the acceleration in the z-axis is shown for an elevator going down two floors. The frequency of this elevator's motor is approximately 150 Hz, therefore, we would need to sample at 300 Hz.

We noticed that the bandwidth needed for going upstairs is slightly smaller than for going downstairs. This is valid for escalators and for staircases as well.

III. Bias Error Analysis

Since the position estimate is highly dependent of the drift of gyroscopes and accelerometers, we construct a model of these errors. For deriving the error models we decided to use the Allan variance.

From Section II we have concluded that the sampling frequency should lie between 200 Hz and 300 Hz. Therefore, we have derived models at 200 Hz for three different IMU types: low-cost, medium range and high-end graded.

A. Allan Variance

The Allan variance (also Allan deviation) is a well known method to analyze the random noise processes of inertial sensors [11]. In a nutshell, the Allan variance analysis shows noise deviation over different length in time of averaged data in a double logarithmic chart. At first, a sequence of data, e.g. of several hours or days, is recorded in a static environment, in terms of signal and temperature, in order to observe the long- and the short-term noise processes. This data is divided into several subsequences of the same length and the average is computed for each subsequence. Afterwards the Allan variance is calculated from all averaged values of the subsequences which have the same length. For detailed formulas, see [11]. The subsequence size varies from one sample to about 10% (or less) of the total sequence length, in order to get some statistical significance. The subsequences are directly related to the time by the sampling rate.

The Allan deviation plot is used to determine quantization noise, random walk (white noise), bias instability, rate/velocity random walk and rate ramp [11]. These different parameters can be observed in different regions of averaged time periods. For low-cost MEMS sensors, random walk and bias instability are most relevant. If the sample rate is high enough, a quantization noise can be observed for low-average time periods.

The Allan deviation plot shows a decreasing trend on the left side of the plot (Figure 7), between 0.01 seconds (one sample if the sampling rate is 100 Hz) and about 10 seconds. In this region, the Gaussian white noise is dominant. The Allan variance of random white noise is reduced by averaging over ever-enlarged sequences. In the center of the plot, the Allan deviation shows a change in the trend. This region is the part where the drift, i.e. the slow changing bias becomes dominant. The bias stability (BS) is located at the minimum (Figure 7). The right side of the plot shows the very slow processes, such as rate or velocity random walk which need a very long sequence of data in order to get repeatable results.

It should be noted that especially MEMS sensors show noise variation at different temperatures. A changing environment temperature, which happens often over several minutes or hours, might result in an increasing slope of the Allan deviation on the right part of the plot (larger times). So it is important to maintain a static temperature during data recording for the Allan deviation plot.

B. Sensor Error Model

The IMU measurements can be represented as

$$x_k = x_{k_{real}} + e_k. \tag{1}$$

being $x_{k_{real}}$ the true value and e_k the measurement error.

The error of the measurement can be decomposed in two errors

$$e_k = \underbrace{b_k}_{\text{bias}} + \underbrace{v_k}_{\text{sensor noise}} . \tag{2}$$

where b_k is the bias error due to the drifting sensors and v_k is the sensor noise that can be considered as gaussian white noise.

To determine the bias error we choose an auto-regressive model (AR) of order one, as it is a suitable model for a random walk process [12]. The $AR1$ model is defined as follows:

$$b_k = c \cdot b_{k-1} + n_k. \tag{3}$$

In [13], a Gauss-Markov model was chosen for IMU bias error model. The Gauss-Markov model defines the constant c by the exponent $e^{-\frac{1}{\tau}}$, where τ is the correlation coefficient.

The variance of the noise n_k is defined as

$$\sigma^2_{n_k} = \sigma^2_{bias} \cdot \left(1 - e^{-\frac{2}{\tau}}\right), \tag{4}$$

where σ_{bias} is the noise of the bias, [14].

We will use the Allan variance for extracting these three parameters, namely sensor noise variance $\sigma^2_{v_k}$, bias noise variance σ^2_{bias} and the correlation coefficient τ.

C. Identification of Error Parameters

The sensor error parameters σ_{v_k}, σ_{bias} and τ can be identified from the Allan deviation plot [15].

1) Sensor Noise σ_{v_k}: The value of the white noise of the sensor can be directly identified in the Allan deviation plot (Figures 8, 9 and 10) by intersecting the curves at 1 second.

2) Correlation Coefficient τ: The correlation coefficient τ is identified over the BS (see Figure 7). We have to identify the point where the Allan deviation curve becomes flat. Then, τ is the number of samples where the BS occurs. This is the point in time from the Allan deviation plot times the sample rate:

$$\tau = t_{BS} \cdot f_s. \tag{5}$$

3) Bias Noise σ_{bias}: The bias noise is calculated by the formula

$$\sigma_{bias} = \frac{BS}{\sqrt{\tau}}. \tag{6}$$

As an example we show in Figure 7 an idealized Allan deviation plot for an accelerometer in red and in blue the Allan deviation plot computed for a simulation of the sensor error model using the derived parameters from the idealized plot. The simulation is achieved by Equations (2) and (3), using a defined value for τ and drawing samples of two independent normal distributions with the variances $\sigma^2_{v_k}$, and σ^2_{bias}. We have generated the model for every sensor in order to check the parameters matching.

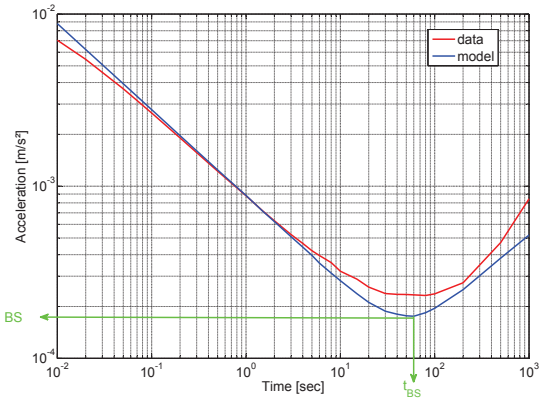

Fig. 7. Example of Allan deviation plot for a real data (red curve) and the modeled data (blue curve). We generate a model for every Allan deviation plot using their derived parameters in order to check the matching between both curves.

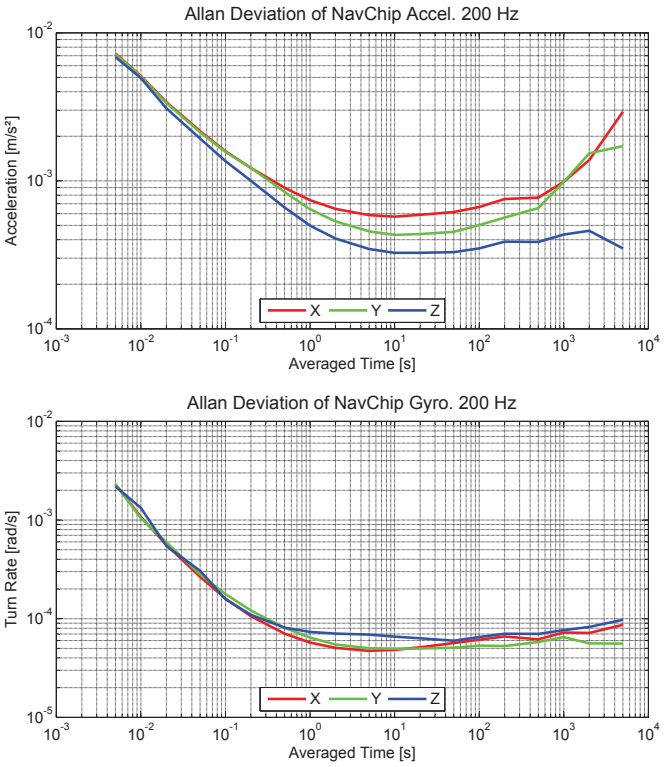

Fig. 8. Allan deviation of all signals from accelerometers and gyroscopes for the InterSense sensor NavChip sampled at 200Hz over 10 hours.

D. MEMS IMU Allan Deviation Study

Figure 8 shows an Allan deviation plot of the NavChip sensor [16] at 200 Hz over 10 hours. Figure 9 shows the same plot for the Xsens sensor MTx [17] at 200 Hz over 12 hours and Figure 10 shows the Allan deviation for the Shimmer sensor [18] at 200 Hz over 3 hours.

Tables IV,V and VI show the identification results of the data of Figures 9, 8 and 10 respectively.

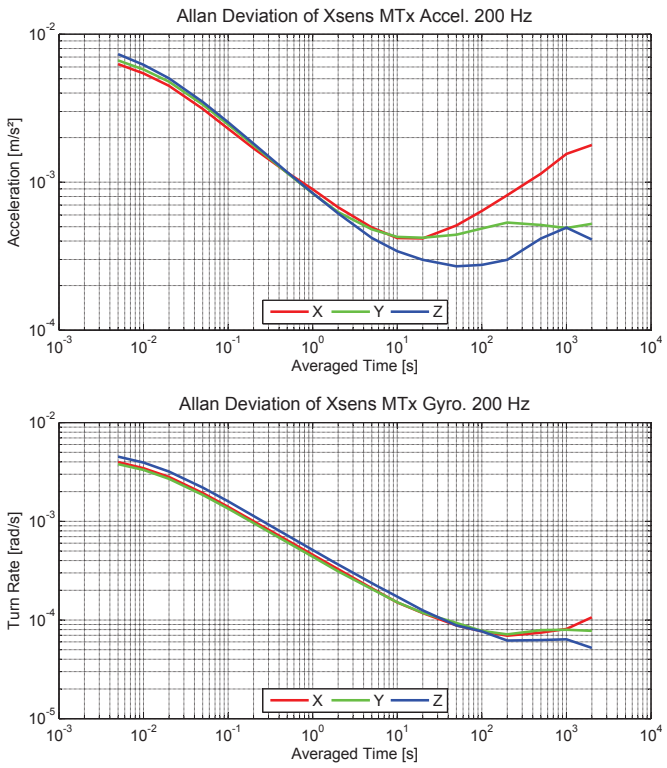

Fig. 9. Allan deviation of all signals from accelerometers and gyroscopes for the XSens sensor MTx sampled at 200Hz over 12 hours.

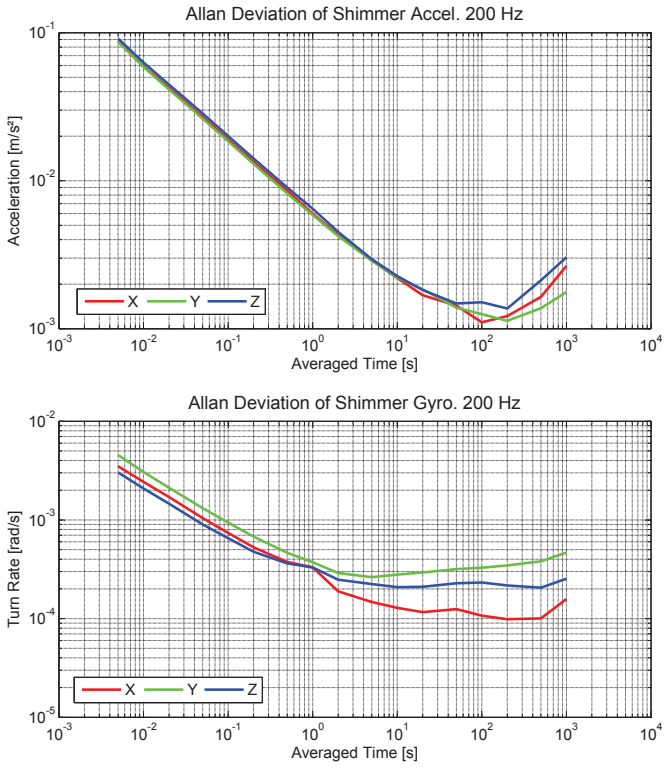

Fig. 10. Allan deviation of all signals from accelerometers and gyroscopes for the Shimmer sensor sampled at 200 Hz over 3 hours.

	Sensor noise σ_{v_k} $[m/s^2/\sqrt{\text{Hz}}\ ,\ ^\circ/s/\sqrt{\text{Hz}}]$	**Corr. coeff.** τ	**Bias noise** σ_{bias} $[m/s^2, ^\circ/s]$
Acc_x	$7.4 \cdot 10^{-4}$	2000	$1.3 \cdot 10^{-5}$
Acc_y	$6.4 \cdot 10^{-4}$	2000	$9.7 \cdot 10^{-6}$
Acc_z	$5.0 \cdot 10^{-4}$	2000	$7.3 \cdot 10^{-6}$
Gyr_x	$3.3 \cdot 10^{-3}$	1000	$8.5 \cdot 10^{-5}$
Gyr_y	$3.7 \cdot 10^{-3}$	1000	$6.4 \cdot 10^{-5}$
Gyr_z	$4.2 \cdot 10^{-3}$	10000	$3.4 \cdot 10^{-5}$

TABLE IV
MODEL PARAMETERS FOR THE INTERSENSE IMU NAVCHIP AT 200 HZ.

	Sensor noise σ_{v_k} $[m/s^2/\sqrt{\text{Hz}}\ ,\ ^\circ/s/\sqrt{\text{Hz}}]$	**Corr. coeff.** τ	**Bias noise** σ_{bias} $[m/s^2, ^\circ/s]$
Acc_x	$8.9 \cdot 10^{-4}$	2600	$7.9 \cdot 10^{-6}$
Acc_y	$8.4 \cdot 10^{-4}$	2600	$8.1 \cdot 10^{-6}$
Acc_z	$8.4 \cdot 10^{-4}$	11000	$2.5 \cdot 10^{-6}$
Gyr_x	$2.6 \cdot 10^{-2}$	42000	$1.8 \cdot 10^{-5}$
Gyr_y	$2.5 \cdot 10^{-2}$	56000	$1.6 \cdot 10^{-5}$
Gyr_z	$2.9 \cdot 10^{-2}$	144000	$8.4 \cdot 10^{-6}$

TABLE V
MODEL PARAMETERS FOR THE XSENS IMU MTX AT 200 HZ.

	Sensor noise σ_{v_k} $[m/s^2/\sqrt{\text{Hz}}\ ,\ ^\circ/s/\sqrt{\text{Hz}}]$	**Corr. coeff.** τ	**Bias noise** σ_{bias} $[m/s^2, ^\circ/s]$
Acc_x	$6.0 \cdot 10^{-3}$	14600	$8.7 \cdot 10^{-6}$
Acc_y	$5.9 \cdot 10^{-3}$	36000	$5.3 \cdot 10^{-6}$
Acc_z	$6.5 \cdot 10^{-3}$	9400	$1.4 \cdot 10^{-5}$
Gyr_x	$1.9 \cdot 10^{-2}$	4200	$1.0 \cdot 10^{-4}$
Gyr_y	$1.7 \cdot 10^{-2}$	800	$5.3 \cdot 10^{-4}$
Gyr_z	$1.9 \cdot 10^{-2}$	2800	$2.2 \cdot 10^{-4}$

TABLE VI
MODEL PARAMETERS FOR THE SHIMMER IMU AT 200 HZ.

IV. INERTIAL NAVIGATION FOR INDOOR POSITIONING

In this work we apply inertial navigation in indoor environments using sequential Bayesian positioning estimators [4]. In particular we have implemented an unscented Kalman filter (UKF) with an integrated strapdown algorithm for computing the final position, like in [6].

The UKF has 15 states: 3 Euler angles, 3-axis velocity, 3-axis position and biases for gyroscopes and accelerometers. The UKF measures the evolution of the states and the influence of the measurements. We can differentiate two steps in the filter: the unscented transformation (UT) that estimates the propagation of the states through sigma points, and the update that corrects the states with the information of the measurements. More details about the UKF can be found in [6].

During the UT step the states are propagated using the information of the strapdown algorithm [1]. This algorithm takes directly the raw signals provided by the 3 orthogonal accelerometers and gyroscopes. The integration of the turn rate signal gives the orientation of the IMU and the final position estimation is computed through the double integration of the given acceleration information. During the update step the measurements correct the states estimations. In our case we use only the ZUPT pseudo-measurements.

In the following section we will evaluate the odometry. To illustrate the benefit of the developed bias model, we will process the same dataset using the model and without using it. We will keep the already described 15 states UKF for both cases.

A. Without the Bias Model

In all cases, before starting the walk, we keep standing a couple of seconds at the initial position without moving. This is necessary for calibrating the initial alignment of the IMU once it is attached to the foot. Under the assumption that the user is not moving, all the fluctuations the IMU senses are due to the biases.

When we do not use the model, we compute the initial biases of accelerometers and gyroscopes in the alignment stage and we keep this value for the whole walk. We use 0 for the noise of the bias in the covariance matrix Q (see [6] for UKF details).

B. With the Bias Model

In the case we use the bias model, we use as initial value of the bias the one computed in the alignment stage, the same procedure as when we do not use the model.

We predict with Equation (3) by using the resulting value of Equation (4) for the noise of the bias in the covariance matrix Q (see [6] for UKF details).

V. Evaluation of the Odometry

We have done a set of realistic walks at the Barajas airport in Madrid including elevators, escalators and moving walkway systems. We did as well such walks in our office building using staircases.

We want to compare the performance of different sampling frequencies and evaluate the developed bias model. Therefore, we have chosen a walk done in our office building. We have superposed the floor plan to the $2D$ odometry generated by our UKF explained in Section IV.

In Figure 11 we can see the walk's trajectory: We started at the third room in the bottom left corner of the floor plan in the second floor, we turned left and walked until the end of the corridor. There we turned around and we crossed to the other side of the building. Then we went to the staircases and went two floors upstairs. The green line represents the walk on the fourth floor, where we went through the kitchen until the opposite staircases. We went two floors downstairs until the second floor again. Finally we turn right until the end of the corridor and finished in the same room as we started.

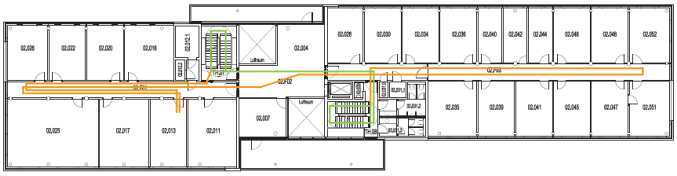

Fig. 11. Trajectory of the walk made by the user. The orange line represents the walk in the second floor and the green line represents the walk in the fourth floor. The starting and the ending point are situated at the third room in the bottom left corner.

A. Evaluation of the Bias Model

We have done the same walk described in Figure 11 at 200 Hz sampling frequency. First we have used the InterSense IMU Navchip and we have analyzed the obtained dataset without and with the bias model as we have described in Subsections IV-A and IV-B. Figure 12 shows the odometry with the floor plan of our office building superposed and Figure 13 shows the z-component.

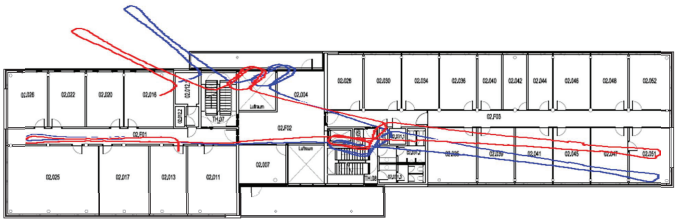

Fig. 12. Odometry for the NavChip IMU for the trajectory described in Figure 11 sampled at 200 Hz. The blue curve represents the output of the data computed without using the biases model and the red line represents the output of the data computed using the model.

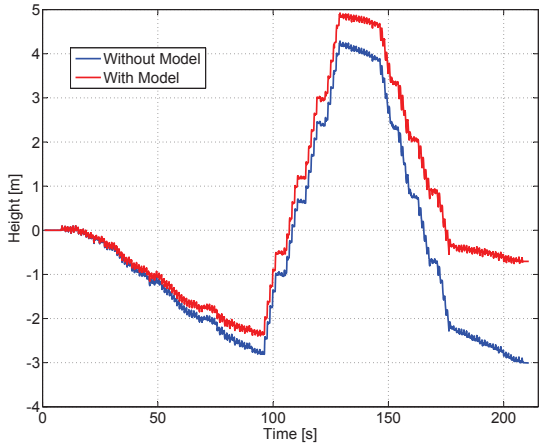

Fig. 13. Z-component trajectory for the NavChip IMU for the walk described in Figure 11 sampled at 200 Hz. The blue curve represents the output of the data computed without using the biases model and the red line represents the output of the data computed using the model.

We have also done the walk described in Figure 11 with the Xsens MTx IMU at 200 Hz sampling frequency. Figure 14

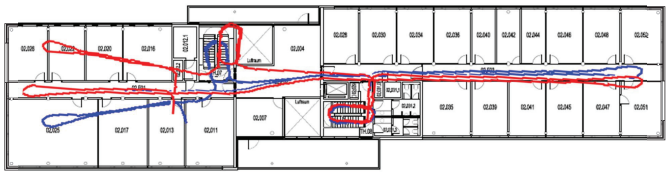

Fig. 14. Odometry for the MTx IMU sampled at 200 Hz for the trajectory described in Figure 11. The blue curve represents the output of the data computed without using the biases model and the red line represents the output of the data computed using the model.In this plot the blue and red curves are completely superposed at the beginning of the walk.

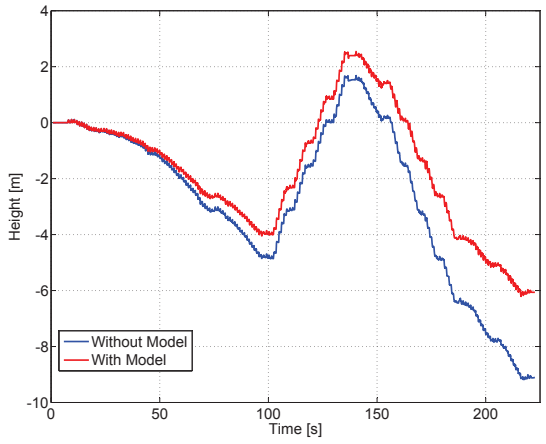

Fig. 15. Z-component trajectory for the MTx IMU for the walk described in Figure 11 sampled at 200 Hz. The blue curve represents the output of the data computed without using the biases model and the red line represents the output of the data computed using the model.

Fig. 16. Odometry for the NavChip IMU for the trajectory described in Figure 11. The blue curve represents the output of the data computed using the biases model sampled at 100 Hz and the red line represents the output of the data computed using the model sampled at 200 Hz.

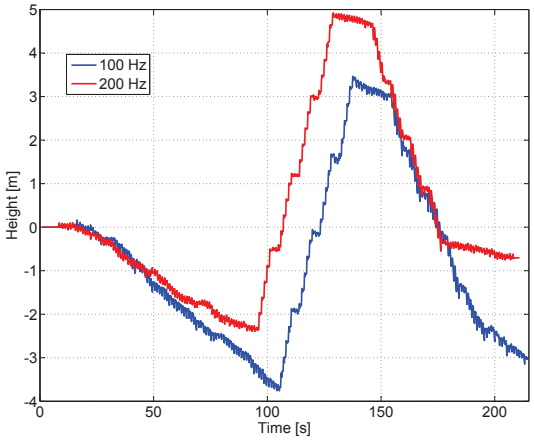

Fig. 17. Z-component trajectory for the NavChip IMU for the walk described in Figure 11. The blue curve represents the output of the data computed using the biases model sampled at 100 Hz and the red line represents the output of the data computed using the model sampled at 200 Hz.

shows the odometry with the floor plan superposed and Figure 15 shows the z-component.

In general for both IMUs we can observe a better behaviour when we compute the generated dataset using the bias model (curves represented in red). For the odometry the curves representing the dataset computed with the model are slightly better. The extra difficulty of this walk is the 2 floors up- and downstairs. Keeping the correct heading after the staircases than before is one of the advantages of the model. For the z-component the corrections made by the bias model are easier to recognize. With the NavChip sensor we got more than 2 meters less drift after a walk longer than 3 minutes using staircases. For the MTx we got a 3 meters drift correction.

B. Evaluation of the lowest usable sampling frequency

In this case we have kept the bias model on. To illustrate the effect of using a sampling frequency lower than the lowest usable sampling frequency, we have done the same walk described in Figure 11. We have sampled at 100 Hz and then at 200 Hz.

First we show the results obtained with the NavChip IMU. In Figure 16 the odometry is shown with a superposed floor plan of our office building. Figure 17 shows the z-component. We plot the curve representing the dataset sampled at 100 Hz with a blue line and the dataset sampled at 200 Hz with a red curve.

We have applied the same procedure with the MTx IMU. In Figure 18 is represented the odometry with a superposed floor plan and Figure 19 shows the z-component. For both cases we have computed the datasets at 100 Hz and 200 Hz using the bias model and we have represented the results at 200 Hz with the red curves.

For the NavChip the odometry results are slightly better at 200 Hz. We can better evaluate these results focusing on the heading. The critical situations are the ones after the 360° curves and after the staircases. However, in this case the performance at both sampling frequencies is similar. The really clear result is shown for the z-component (Figure 17). Only

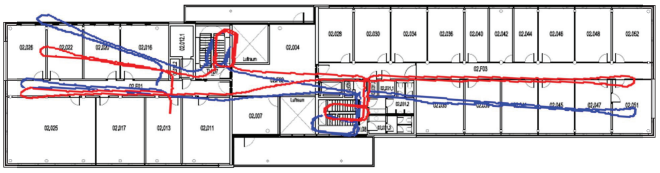

Fig. 18. Odometry for the MTx IMU for the trajectory described in Figure 11. The blue curve represents the output of the data computed using the biases model sampled at 100 Hz and the red line represents the output of the data computed using the model sampled at 200 Hz.

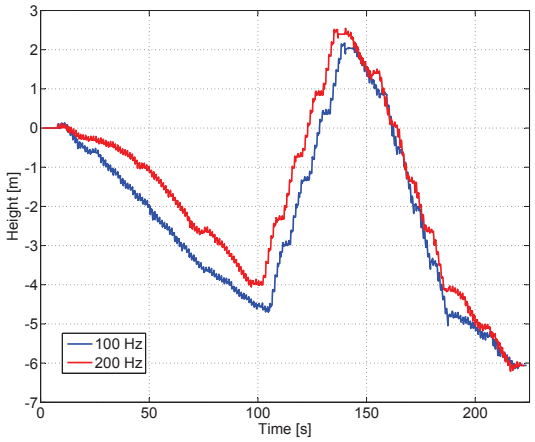

Fig. 19. Z-component trajectory for the MTx IMU for the walk described in Figure 11. The blue curve represents the output of the data computed using the biases model sampled at 100 Hz and the red line represents the output of the data computed using the model sampled at 200 Hz.

by sampling at 200 Hz we got 2 meters less drift after a walk longer than 3 minutes.

For the MTx the results are more clear in the odometry. As we can see in Figure 18, the blue curve which represents the dataset recorded at 100 Hz has considerably more drift when walking in a straight line for long distances. This drift is constant and we can see a more corrected drift in the red curve. In Figure 19 we got a 1 meter constant less drift only by sampling at 200 Hz, however it seems like this advantage is lost within the last 30 seconds of the walk.

The results obtained in this work about the required sampling frequency for a foot-mounted IMU are promising. For the rest of the walks we have done, the general behaviour of the shown plots is repeated.

It is still under investigation the behaviour of the drift for the z-component. For most of the cases we have obtained always a negative drift and only few walks have resulted in a positive drift. It is still being investigated how the drift changes when going up- and downstairs.

VI. Conclusions

The objective of this work is to increase the accuracy of the position estimate for foot-mounted IMUs. Therefore, we have decided first to investigate on the lowest usable sampling frequency and second to derive an error model for the biases of accelerometers and gyroscopes for compensating their drift.

For the first part we have studied different motions, kind of floors and footwear. We have found that the lowest usable sampling frequency lies between 200 Hz and 300 Hz. We have made a set of walks for proving the importance of sampling at the correct rate and the results show a more reduced error only by sampling at 200 Hz instead of 100 Hz.

For the compensation of the sensors drift we have derived an error model for the biases of accelerometers and gyroscopes. We have made use of the Allan deviation plots for identifying the model parameters. We have made a set of walks in order to illustrate the performance of the odometry with and without using the model. With the biases model we have reduced considerably the positioning error.

References

[1] D. Titterton and J. Weston, *Strapdown Inertial Navigation Technology*, 2004.

[2] S. Rajagopal, "Personal Dead Reckogning System with Shoe Mounted Inertial Sensors," Ph.D. dissertation, 2008.

[3] E. Foxlin, "Pedestrian Tracking with Shoe-Mounted Inertial Sensors," *IEEE Computer Graphics and Applications*, pp. 38–46, December 2005.

[4] B. Krach and P. Robertson, "Cascaded Estimation Architecture for Integration of Foot-Mounted Inertial Sensors," *Location and Navigation Symposium IEEE/ION*, 2008.

[5] A. Jimenez, F. Seco, J.Prieto, and J.Guevara, "A Comparison of Pedestrian Dead Reckoning Algorithms Using a Low-Cost MEMS IMU," *IEEE International Symposium on Intelligent Sygnal Processing*, pp. 37–42, August 2009.

[6] F. Zampella, M. Khider, P. Robertson, and A. Jimenez, "Unscented Kalman Filter and Magnetic Angular Rate Update (MARU) for an Improved Pedestrian Dead-Reckoning," *Position Location and Navigation Symposium (PLANS) IEEE/ION*, 2012.

[7] T. Jost, M.Khider, and E. Abdo Sanchez, "Characterisation and Modelling of the Indoor Pseudorange Error using Low Cost Receivers," *ION ITM, San Diego, USA*, January 2010.

[8] C. Gentner, J.-M. Rawadi, E. Munoz Diaz, and M. Khider, "Hybrid Positioning with 3GPP-LTE and GPS Employing Particle Filters," *Proceedings of ION GNSS*, 2012.

[9] M. Khider, "Implementation of a Simulator/Demonstrator for the Soft-Location Concept Using Bayesian Filters," 2005.

[10] P. H. J-O Nilsson, I. Skog, "Performance characterisation of foot-mounted ZUPT-aided INSs and other related systems," *International Conference on Indoor Positioning and Indoor Navigation*, September 2010.

[11] "IEEE Standard Specification Format Guide and Test Procedure for Single-Axis Interferometric Fiber Optic Gyros," *IEEE Std 952-1997*, 1998.

[12] S. Kay, *Fundamentals of Statistical Signal Processing: Estimation Theory*, ser. Prentice Hall Signal Processing Series. Prentice Hall, 1993, no. Bd. 1.

[13] D. Gebre-Egziabher, "Design and Performance Analysis of a Low-Cost Aided Dead Reckoning Navigator," Ph.D. dissertation, Stanford University, USA, feb 2004.

[14] M. El-Diasty and S. Pagiatakis, "Calibration and stochastic modeling of inertial navigation sensor errors," *Journal of Global Positioning Systems*, vol. 7, no. 2, pp. 170–182, 2008.

[15] O. J. Woodman, "An Introduction to Inertial Navigation," *Technical Report. Number 696. University of Cambridge*, August 2007.

[16] InterSense NavChip IMU. [Online]. Available: http://www.intersense.com/pages/16/16

[17] Xsens MTx IMU. [Online]. Available: http://www.xsens.com/en/general/mtx

[18] Shimmer Wireless 9DoF IMU Sensor. [Online]. Available: http://www.shimmersensing.com/shop/wireless-9dof-imu-sensorspecifications-tab